ICRF Edge Modeling Studies

CONF-8910225--6

DE90 006644

Ira S. Lehrman
Grumman Corporate Research Center
Princeton, NJ 08540
USA

Patrick L. Colestock
Princeton Plasma Physics Laboratory
Princeton, NJ 08543
USA

Presented at the
IAEA Technical Committee Meeting on ICRH / Edge Physics
October 2-5, 1989, Garching, FRG

Abstract

Theoretical models have been developed, and are currently being refined, to explain the edge plasma-antenna interaction that occurs during ICRF heating. The periodic structure of a Faraday shielded antenna is found to result in strong ponderomotive force in the vicinity of the antenna. A fluid model, which incorporates the ponderomotive force, shows an increase in transport to the Faraday shield. A kinetic model shows that the strong antenna near fields act to increase the energy of deuterons which strike the shield, thereby increasing the sputtering of shield material. Estimates of edge impurity harmonic heating show no significant heating for either in or out-of-phase antenna operation. Additionally, a particle model for electrons near the shield shows that heating results from the parallel electric field associated with the fast wave. A quasilinear model for edge electron heating is presented and compared to the particle calculations. The models' predictions are shown to be consistent with measurements of enhanced transport.

1. Introduction

In recent years, considerable attention has been focused on the ec interaction that occurs during Ion Cyclotron Range of Frequencies (ICR ICRF heating has shown promise for heating plasmas to ignition condi of undesired side effects often accompany the ion heating. The most no increase in the impurity concentration, and an increase in the plasma experiments have reported on the favorable use of wall and antenna cond and in some cases suppress, the deleterious effects of ICRF heatin applicability of such conditioning in reactors is uncertain.

In this paper, edge plasma models previously developed,[6] alc progress is presented. The purpose of these models is to ascertain the processes at work in coupling ICRF power to plasmas. Since experimen identify the energized antennas as significant sources of impurities and models presented simulate the particle transport in the vicinity of the ante kinetic modifications of the edge plasma and their implication on materia the Faraday shield are investigated.

The electric fields produced by the antenna are computed using t ORION[9] codes. These fields are then used in conjunction with the models paper. The two-dimensional near-field structure of a Faraday shielded I evaluated. The Faraday shield is shown to induce poloidal ripple in the in electric field (E_y). The ripple in the near field is found to result in strong force acting mainly on the ions. A fluid model that incorporates the ponde indicates that the transport of particles to the Faraday shield is enhanced abo level.

Additionally, kinetic models are presented that determine the energy ions and electrons close to the shield. The average energy of deuterons in the Faraday shield is found to be significantly increased, while harmonic he

a: .. carbon is found to be negligible for both in and out-of-phase operation of the double-loop an.e.nas. Calculations of particle trajectories in the edge region find that the parallel electric ($E_{||}$) field, induced as a result of plasma operation, modifies the electron distribution. A quasilinear model of edge electron heating is also presented.

2. Structure of the Antenna Near Field

In order to accurately model the edge plasma-antenna interaction, an accurate determination of the near field close to the Faraday shield is required. A number of authors have considered the near-field characteristics of Faraday shielded ICRF antennas.[10,11,12,13] The most important property of a Faraday shield is its ability to suppress the electrostatic field while allowing transmission of the inductive electric field. In this section, an analytic description of the antenna near field in vacuum is presented for thin blade shields.

The metallic boundary condition on the surface of the shield requires that the tangential electric field be identically zero. Since the Faraday shield is not expected to greatly reduce the power radiated from the antenna,[11] the inductive electric field must, on average, be unchanged with the addition of the shield. Therefore, the arrangement of the shield elements acts to geometrically magnify the electric field in the gap region while suppressing the field in the region of the blades. For a typical Faraday shield with 1 cm shields (poloidal extent) and 0.5 cm gaps, the electric vacuum field in the gap region is three times larger than the average electric field.

The two-dimensional structure of the electric field is determined by Fourier analyzing the electric field at the shield surface. The field, analyzed in the poloidal direction (y), is found to be:

$$E_y(x,y) = E_o\left[1 + \sum (A_n \cos(k_{yn}\, y) + B_n \sin(k_{yn}\, y))\, e^{-k_{yn}\, x}\right],$$

where

$$k_{yn} = \frac{2\pi n}{\text{blade spacing}}.$$

with

$$A_n = \frac{2}{s\, k_{yn}} \left[\sin(k_{yn} w/2) - \sin(k_{yn}\,(s-w/2))\right]$$

$$B_n = \frac{-2}{s\, k_{yn}} \left[\cos(k_{yn} w/2) - \cos(k_{yn}\,(s-w/2))\right],$$

where s is the spacing between adjacent shield blades, and w is the width of the shield blades. Since $k_{y1} >> k_o$, the ripple in the field is evanescent, decaying in about a shield spacing. The complete field structure for a 250 V/cm electric field incident on the Faraday shield is shown in Figure 1. Since the lowest order mode expected to be supported by the plasma is much less than k_{y1}, the evanescent near field structure is virtually unchanged in the presence of plasma.[14]

The plasma does influence the component of the electric field parallel ($E_{||}$) to the magnetic field (B_0). The ORION code was used to determine $E_{||}$ in the vicinity of the antenna. For typical tokamak edge parameters, $E_{||} \approx 10^{-5}\, E_y$. When the Faraday shield elements are included in the calculation, $E_{||} = 0.02\, E_y$, significantly enhanced over the case of no shield. This is a result on charge accumulation on the shield blades. It should be noted that $E_{||}$ is not equal to $B_p/B_t\, E_y$, where B_p and B_t are the poloidal and toroidal magnetic field components, respectively (the gap voltage divided by the length of the field line connecting two blades). This would suggest that $E_{||} = 0.13\, E_y$, a factor of 6 greater than the ORION calculation.

The analysis of the near fields provides models for the antenna field structure which are used in the proceeding sections to investigate the effects of ICRF heating on the edge plasma.

3. Particle Orbits

In this section, particle orbits of electrons and ions are examined to determine if their trajectories result in particle transport. The radial excursion for electrons in the edge can be estimated by the $E_y \times B_o$ drift that they experience from the RF electric field. Electrons, traveling in the gap (high field) region, exhibit the maximum excursion in half an RF period. With 1 MW applied to the TFTR antenna (in-phase), the maximum excursion is less than 0.1 mm. In the next half of the RF period the electron will move back by this amount, hence there is no net radial transport.

The ion trajectory, which is more complicated since $\omega \sim \omega_{ci}$, can not be modeled in this manner. The orbit must be numerically integrated with the spatial variation of the antenna near fields included. Due to the short scale length of the ripple in the antenna near field, an RF component of magnetic field parallel to the toroidal magnetic field is induced and must be included in the orbit calculation. Figure 2 depicts the trajectory of a deuteron in the antenna region (Fig. 1). The deuteron started at y = 0.6 mm, x = 1 mm and experienced a net drift which carried the particle into the shield region at y = 0.51 mm, x = 0. This drift, which results in net transport, is explained by the ponderomotive force on ions in the vicinity of the antenna.

The ponderomotive force (F_{pi}) is due to a gradient in the magnitude of the electric field, thus the ripple in the near field induced by the Faraday shield results in strong ponderomotive force. Since the ponderomotive force is perpendicular to the magnetic field, a drift results:

$$V_{Di} = \frac{F_{pi} \times B_o}{qB_o^2} .$$

For comparison, this drift is also shown in Fig. 2. Notice that the drift is a good approximation to the actual particle orbit. The ponderomotive force is incorporated into a fluid model in the next section.

4. Fluid Model of the Edge Plasma

In order to obtain a self-consistent model for the edge plasma in the vicinity of the ICRF antenna, the ponderomotive force is incorporated into the ion fluid equations. The ponderomotive force acts mosts strongly on the ions with the electrons responding to any charge imbalance created by local accumulation or depletion of the ions. The solution of the ion fluid equations are used to estimate the particle transport to the Faraday shield.

The fluid equations are averaged over a few periods of the fundamental cyclotron frequency to obtain the steady values. The equation for the perturbed ion velocity is:

$$V_i^{(2)} = \frac{q}{m_i B_o^2} \left[E^{(2)} \times B_o + S_i \times B_o \right] - \frac{\nabla P_i \times B_o}{m_i n_o B_o^2} ,$$

where S_i is the ponderomotive force (multiplied by q/m_i). P_i is the ion pressure and the quasistatic electric field, $E^{(2)}$ is evaluated by requiring that electrons follow Boltzmann's relation:

$$E^{(2)} = \nabla \left(\frac{kT_e}{q} \ln \left[1 + \frac{n_e^{(2)}}{n_o} \right] \right)$$

The perturbed ion density, $n_i^{(2)}$ is evaluated from:

$$\frac{\partial n_i^{(2)}}{\partial t} = - n_o \nabla \cdot V_i^{(2)} - V_i^{(2)} \cdot \nabla n_o - V_i^{(2)} \cdot \nabla n_i^{(2)} - V_z \cdot \nabla n_i^{(2)} + D_\perp \nabla^2 n_i^{(2)},$$

where $n_e^{(2)} \approx n_i^{(2)}$, and $D_\perp$ is the perpendicular particle diffusion coefficient. The perturbed ion velocity, V_z, which accounts for particle flow along field lines, is determined from:

$$V_z = C_s \sqrt{\frac{2\, n_i^{(2)}}{n_o}}$$

where C_s is the ion sound speed. From the solution of the velocity and continuity equations, the ion flux to the Faraday shield is evaluated:

$$\Gamma_x = - n_o V_{ix}^{(2)} - D_\perp \nabla \left(n_i^{(2)} + n_o \right).$$

The fluid model was applied to the edge conditions of the PLT tokamak for the case of 400 kW applied to one of the antennas. An edge density of 1×10^{12} cm^{-3} and $D_\perp$ = 1.25 m^2/s was assumed. The resulting particle flux to the shield surface is shown in Fig. 3. The flux has an asymmetric component since the ponderomotive force points in opposite poloidal directions at the two edges of the shield. The poloidal ponderomotive force results in a radial particle drift. Near one edge of the shield the radial drift is directed into the shield, while on the opposite edge the drift is directed away from the shield. For these parameters, the integrated particle flux to the shield is doubled. The model predicts a linear increase in the particle flux with applied power; consistent with the D_α emission measurements which also exhibit a linear increase with applied power.[7]

Though the fluid model can be used to explain the increased release in deuterium during ICRF heating, the model does however, fail to explain the increase in the metallic release during ICRF heating. The metallic increase is correspondingly larger than the increase in deuterium. Since metallic production is likely due to sputtering from edge ions, the energy distribution of ions that impact the Faraday shield must be investigated.

5. Kinetic Modeling

The sputtering of atoms from metallic surfaces is described by a sputtering yield that determines the number of atoms released per impacting ion. This yield is sensitive to the mass and energy of the impacting ion and the surface material. Ions, which fall through the sheath that forms at boundary surfaces, acquire approximately an additional $3ZkT_e$ of energy (Z is the ionic charge state). Electron heating, therefore, will act to enhance the sheath potential, and hence the energy of the ions which strike the shield. Electron heating is discussed in Sec. 5.2. In Sec. 5.1, the energy distribution of ions in the vicinity of the antenna is determined.

5.1 Ion Kinetics

5.1.1 Deuterium Ion Kinetics

In the gap region of the Faraday shield, the electric field is nearly linearly polarized. To obtain the time evolution of the ion energy, the velocity squared is evaluated,

$$V^2 = V_y^2 + V_x^2$$

$$= V_o^2 + \frac{2\,qV_o\,E_{yo}}{m_i\,(\omega_{ci}^2 - \omega^2)}\left[\omega_{ci}\sin(\omega t + \phi)\sin(\omega_{ci}\,t) + \omega\cos(\omega t + \phi)\cos(\omega_{ci}\,t)\right]$$

$$+ \frac{q^2\,E_{yo}^2}{m_i^2\,(\omega_{ci}^2 - \omega^2)^2}\left[\omega_{ci}^2\sin^2(\omega t + \phi) + \omega^2\cos^2(\omega t + \phi)\right].$$

where ϕ is an arbitrary phase angle associated with the RF. The first term, V_o, is the initial ion velocity. The second term contains oscillatory quantities which time average to zero, while the time average of the last term is non-zero. From the equation for V^2, the time-averaged energy is obtained:

$$\frac{1}{2}m_i\langle V^2\rangle = \frac{1}{2\pi}\int_0^{2\pi}\frac{1}{2}m_i V^2\,d\phi = \frac{1}{2}m_i V_o^2 + \frac{q^2\,E_{yo}^2\,(\omega_{ci}^2 + \omega^2)}{2m_i\,(\omega_{ci}^2 - \omega^2)^2}.$$

The average energy of the ion is now equal to its initial energy plus an additional term known as the quiver energy. The quiver energy represents stored (reactive) energy which is given back as wave energy when the RF is turned off, that is unless the particle suffers a collision or impacts the shield. The quiver energy becomes important in the vicinity of the Faraday shield since the local RF electric field is magnified by the shield structure. For the field structure of Fig. 1, an electric field of 250 V/cm results in a quiver energy of 12.6 eV for deuterium ions in the gap region (750 V/cm).

The RF acts to broaden the distribution of particle in velocity space with the net result being an increase in the average energy of the distribution. To calculate the change in the distribution function induced by the RF, a Maxwellian distribution of ions is introduced into the RF field and the particles are then sampled to determine the distribution shown in Fig. 4a. The average energy of the RF distribution is found to be 21.8 eV, which is nearly

equal (calculation accuracy) to the initial energy (10 eV) plus the quiver energy (12.6 eV). Also shown in Fig. 4a are Maxwellians of 10 eV and 21.8 eV for comparison. The probability distribution function, $V_\perp f(V_\perp)$, shown in Fig. 4b, indicates that the RF acts to push particles away from the lower energies.

With a knowledge of the energy distribution of particles that impact the shield, an estimate of the sputtering yield can be made. Roth[15] studied the sputtering of metals by light ions and has proposed a general formula for the sputtering yield from atomic elements. Using the RF ion distribution function, curves of yield versus RF electric field are constructed. Figure 5a and b) show the sputtering yield from deuterium ion distributions with initial energies of 10 and 20 eV, respectively. Each curve is labelled by a possible sheath potential which ions might acquire as they impact the shield surface. The yield curves show that the quiver energy can significantly increase the number of impurity atoms that are released during ICRF heating.

5.1.2 Impurity Ion Kinetics

It has been suggested by Puri[16] that harmonic heating of edge impurities could be responsible for the observed impurity production during ICRF heating. In particular, Puri calculated analytically 3rd harmonic heating of carbon ions in the 5th charge state. It is not unexpected that C^{5+} does exist in the edge region since the diffusion and energy equilibration times are fast compared to the time for recombination.[17]

In order to reproduce Puri's result, the toroidal variation of the TFTR double-loop antenna was determined for in and out-of-phase operation. The electric field is determined by spatial integration of Faraday's law from the surface of the current strap. Since the field lines are tilted by about 0.1 radians from the axis of the shield blades, a field line crosses approximately 5 gaps in traversing the 54 cm wide antenna. The electric field (E_y) along a field line 1 cm in front of the TFTR antenna for in and out-of-phase operation is shown in Fig. 6. Notice that the magnitude of the peak electric field is not much different for the two

phasings. Although in-phase operation results in a larger loading resistance than out-of-phase operation, he inductance is also greater, hence the inductive electric field for a given power is not much different.

Particle trajectories of C^{5+} and He (5^{th} Harmonic) have been integrated to determine if significant harmonic heating would result. No significant heating was observed for the two phasing or species examined. In addition, experimental measurements on TFTR indicate no change in the spectroscopic emission at the antenna when the toroidal field was varied by a few kilogauss, enough to shift the location of the impurity resonances off the antenna.[18] Puri did not consider the toroidal variation of the electric field and assumed that all of the RF field energy was in the left-circularly polarized wave component, when in fact, the wave can be greater than 50% right-circularly polarized in the edge region.[14]

5.2 Electron Kinetics

5.2.1 Particle Calculation

Experimental measurements on the PLT tokamak indicate that in flux tubes that lie close to the surface of the Faraday shield, electron heating occurs.[7] To explain the observed heating, electron trajectories (~10,000) are followed past the antenna. The distribution of electrons is then computed. Since the perpendicular components of the electric field are expected to negligibly affect the electron energy (quiver energy << kT_e/e), the effect on electrons from $E_{||}$ only is investigated.

Due to the tilt of the magnetic field lines, the toroidal variation of $E_{||}$ is modeled as a gap field of the form:

$$E_{||}(z) = \frac{E_{||o}}{2}\left[\tanh\left(\frac{z-l/2}{s} \right) - \tanh\left(\frac{z+l/2}{s} \right) \right],$$

where s is a shape factor and l is equal to the toroidal projection of the field line between the shield elements (5 cm). $E_{\|o}$ decayed nearly exponentially from 12 V/cm at the shield surface with an e-folding length of 1 cm. Figure 7 shows the electron distribution that results for $E_{\|} = 5$ V/cm and $s = 0.1$ cm.

We note that the number of slow electrons is reduced because the RF acts to accelerate these particles up to a velocity at which they can transit the antenna in approximately one RF period. Particle with velocities near 1.5×10^6 m/s fall into this category. Particles which transit the antenna in less than one RF period, but greater than half an RF period, may be either slowed or accelerated depending upon the phase of the RF. Fast particles, those that pass the antenna in less than half an RF period, have an equal probability of being slowed or accelerated. Since the initial distribution is monotonically decreasing, the net effect is to increase the number of fast particles.

To model the electron heating observed in the PLT experiments, the electron distributions were computed for a range of spatial positions. From the resulting distributions the average parallel electron energies $\langle W_{\|} \rangle$ were computed. Since collisions between successive antenna transits act to equate the parallel and perpendicular energy distributions, the predicted electron temperature is taken to be:

$$T_e = \frac{\langle W_{\|} \rangle + 2T_{\perp}}{3} .$$

Figure 8 shows the experimentally measured change in T_e along with the predicted change in T_e for the three different shape factors. Within the experimental error of the measurements, the agreement suggests that $E_{\|}$ induced at the shield surface is responsible for the observed electron heating. This increase in electron temperature is of great concern since it can result in an increase in the sheath potential, and thus sputtering, at the Faraday

shield surface. This analysis has not yet been extented to evaluate the effect of antenna phasing.

5.2.2 Quasilinear Theory for Electron Heating

With the use of quasilinear theory we derive a quasilinear operator for electron heating in the edge region. Since the $E_{||}$ field can be represented by a pulse in space, its Fourier representation is easily found:

$$E_{||}(k) = E_{||o} l \frac{\sin(k\, l/2)}{k\, l/2}.$$

We start by assuming that the evolution of the distribution is slow compared to the RF frequency and determine the quasilinear operator.

$$\left.\frac{\partial f}{\partial t}\right|_{slow} = \frac{-i}{2\pi} \frac{q^2}{m^2} \frac{\partial}{\partial V} \int E_k F_{-k} \frac{\partial f}{\partial V} \frac{1}{\omega - kV}\, dk$$

In order to perform the integration, we substitute $E_k E_{-k} = E_{||o}^2 l^2 \,\mathrm{sinc}^2(k\, l/2)$, where $\mathrm{sinc}(x) = \sin(x)/x$. We now have

$$\left.\frac{\partial f}{\partial t}\right|_{slow} = \frac{-i}{2\pi} \frac{q^2}{m^2} \frac{\partial}{\partial V} \int E_{||o}^2 l^2 \,\mathrm{sinc}^2(k\, l/2) \frac{1}{V} \frac{\partial f}{\partial V} \frac{1}{\omega/V - k}\, dk$$

The single pole at $k = \omega/V$ simplifies the integration;

$$\left.\frac{\partial f}{\partial t}\right|_{slow} = \frac{q^2}{2m^2} E_{||o}^2 l^2 \frac{\partial}{\partial V} \left[\mathrm{sinc}^2\left(\frac{\omega\, l}{V\, 2}\right) \frac{1}{V} \frac{\partial f}{\partial V} \right]$$

We desire the steady state solution to the distribution function, therefore $\partial f/\partial t$ is set equal to zero and collisions are introduced in order to balance the effect of the RF.[19] This results in a first-order differential equation for f:

$$\frac{\partial f}{\partial V} = -\frac{2V\,(m_e/m_B)\,\alpha_B^2\,G(\alpha_B V)\,\Gamma_B}{G(\alpha_B V)\,\Gamma_B + C\,\mathrm{sinc}^2\left(\frac{\omega l}{V\,2}\right)}\,f$$

$$= -\beta(V)\,f$$

where

$$\alpha_B^2 = \frac{m_B}{2kT_B} \qquad \Gamma_B = \frac{q_e^2\,q_B^2\,n_B\,\Lambda}{\varepsilon_0\,m_e^2}$$

$$G(u) = \frac{\Phi(u) - u\Phi'(u)}{u^2} \qquad C = \frac{q_e^2}{m_e^2}\,E_{\|0}^2\,l^2$$

The subscript B indicates the background species, Λ is the Coulomb logarithm, and Φ is the error function. The solution to f is found from:

$$f(V) = A\,\exp\left[-\int_0^V \beta(V')\,dV'\right]$$

Two difficulties of particular importance come into play regarding this solution method. First, the $\mathrm{sinc}^2(1/V)$ dependence of β makes the integration difficult, if not impossible, near $V = 0$. Second, the slow particles of the distribution may be trapped in the wave field or

may be accelerated by a significant fraction of their thermal speed in an RF period, both of which violate the restrictions put on quasilinear theory. Particles with velocities

$$V \approx \frac{q}{m}\frac{E_{\|o}}{\omega}\sqrt{8}$$

fall into this category. Since we do not have a method for dealing satisfactorily with these slow particles, β was redefined to be:

$$\beta(V)\left[1 - e^{-4V^2/V_{th}^2}\right]$$

so that the slow particles would be unaffected by the RF. This allows the equation for f to be solved numerically. Figure 9 shows the distribution that results for $E_{\|o} = 2 \times 10^{-4}$ V/cm along with a 20 eV Maxwellian. The quasilinear calculation exhibits similarities to the particle calculation (Fig. 7), although the electric field was 25,000 times smaller. The quasilinear calculation suggests that the distortion of the distribution is greater for a number of reasons. The slow particles are not addressed, the collision operator does not account for the rapid loss of particles to the limiter, and a particle source is not included. Future development will attempt to incorporate a diffusion operator for trapped particles. The trapped particles will on average be pushed to higher velocities thus reducing the number of slow particles as the calculation of Sec. 5.2.1 suggests.

6. Discussion

The models presented in this paper have attempted to explain some of the changes observed in ICRF heating experiments. By considering the results of the fluid and kinetic modeling in conjunction, the following scenario has been applied to the PLT experiments.

The fluid model indicates that the particle flux to the antenna is increased by a factor of two. As a result of the $E_{||}$ field at the antenna, the sheath potential may be increased by as much as 25 eV. To estimate the change in sputtering, the ohmic plasma is assumed to have an electron temperature of 15 eV (-45 V sheath potential) and an ion temperature of 10 eV. The sputtering yield, referring to Fig. 3 is 7×10^{-4} atoms/ion. During the ICRF heated phase of the discharge, the ion temperature increases from 10 to 20 eV due to an increase of heat flow in the edge and the sheath potential is increased to - 70 V, due to $E_{||}$. The sputtering yield is raised to 3.8×10^{-3} atoms/ion, an increase of a factor of 5.4 above the ohmic level. Since the particle flux is also doubled, the net effect is a factor of 10.8 in sputtering yield above the ohmic level. Experimental measurements indicated a factor of 8 increase in chromium during ICRF heating, in line with modeling predictions.

The models, though plausible, can not be used to determine exactly the impurity release during ICRF heating, but should instead be used to predict the relative importance of the various edge processes that occur during ICRF heating. In this vein, the magnitude of the antenna electric field must be reduced in order to limit the production of impurities. This reduction can be most easily achieved by improving antenna coupling. The model also suggests that the gap to blade width ratio should be increased in order to reduce the ponderomotive forces near the shield.

Acknowledgements

This work was supported by the Grumman Corporation under United States Department of Energy (USDOE) contract # DE-FG02-86ER53236, and Princeton University under USDOE contract # DE-AC02-76CHO3073.

References

[1]*e.g.* IAEA Technical Committee Meeting on ICRH/Edge Physics, Garching, FRG, Oct. 2-5,1989; Workshop on Particle Simulation of the Edge Plasma for ICRF Heating, Boulder, CO. Jan. 26-27, 1989; ICRF Edge Physics Meetings, Boulder, CO. Mar. 30-Apr. 1, 1988 and Oak Ridge, TN. Oct. 6-7, 1987.

[2]J. Jacquinot, Plasma Phys. Contrl. Fusion **30** (1988) 1467.

[3]J. Adam, Plasma Phys. Contrl. Fusion **29** (1987) 443.

[4]A. M. Messian, V. P. Bhatnagar, T. Delvigne, *et al.*, Plasma Phys. Contrl. Fusion **28** (1986) 71.

[5]J.-M. Beuken, L. DeKeyser, T. Delvigne, *et al.*, European Conf. on Contrl. Fusion and Plasma Heating, Dubrovnik (May 1988) 774.

[6]I. S. Lehrman, P. L. Colestock, and E. F. Jaeger, "Edge Modeling of ICRF Heated Plasmas on PLT," submitted to Nuclear Fusion.

[7]I. S. Lehrman, P. L. Colestock, D. H. McNeill, *et al.*, Plasma Phys. Contrl. Fusion (in press).

[8]I. S. Lehrman and P. L. Colestock, IEEE Trans. Plasma Sci. **PS-15** (1987) 285.

[9]E. F. Jaeger, D. B. Batchelor, and H. Weitzner, "Global ICRF Wave Propagation in the Edge Plasma and Antenna Region with Finite $E_{\parallel}$," Nuclear Fusion (in press).

[10]R. R. Weynants, A. M. Messian, C. Leblud, and P. E. Vandenplas, in Heating in Toroidal Plasmas, Como **I** (1980) 487.

[11]D. W. Faulconer, J. Appl. Phys. **54** (1983) 3810.

[12]D. N. Smithe, R. J. Kashuba, T. Kammash, J. Appl. Phys. **59** (1986) 3980.

[13]P. M. Ryan, K. E. Rothe, J. H. Whealton, and D. W. Swain, "Determination of Fields Near an ICRH Antenna Using 3D Magnetostatic Laplace Formulation," in Radio-Frequency Power in Plasmas, AIP: New York (1989) 322.

[14]I. S. Lehrman, "A Study of Coupling and Edge Processes for ICRF Antennas," Ph. D. dissertation, Univ. of Wisconsin (1988).

[15]J. Roth, J. Bohdansky, and W. Ottenberger, "Data on Low Energy Light Ion Sputtering," IPP 9/26, Max Planck Institut Fur Plasmaphysik, Garching (May 1979).

[16]S. Puri, Phys. Rev. Lett. **61** (1988) 959.

[17]R. J. Fonck, M. Finkenthal, R. J. Goldston, *et al.*, Phys. Rev. Lett. **49** (1982) 737.

[18]P. L. Colestock, *et al.*, this conference

[19]T. H. Stix, Nuclear Fusion **15** (1979) 737.

Figure Captions

Figure 1 Antenna near field (E_y) close to the Faraday shield. The average electric field is 250 V/cm.

Figure 2 Ion orbit in the vicinity of the Faraday shield. The ion started 1 mm in front of the shield and drifted into the shield region. Also shown is the pondero-notive drift approximation to the Lorentz orbit.

Figure 3 Resulting particle flux to the shield surface as a result of the ponderomotive force. The ohmic diffusion level is shown for comparison.

Figure 4 a) RF distribution that results when an initial 10 eV Maxwellian distribution of deuterons enter an ICRF field of 750 V/cm. The average energy of the RF distribution is 21.8 eV. A 21.8 eV Maxwellian is shown for comparison. b) RF distributions multiplied by $V_\perp$.

Figure 5 a) Sputtering yield for 10 eV deuterium on Ni including the change of the ion distribution in strong ICRF fields. Each curve is labelled with a possible sheath potential that ions gain as they impact the shield. b) Same as a) except for 20 eV ions.

Figure 6 Toroidal variation of the inductive electric field (E_y) along a field line 1 cm in front of the TFTR double-loop antenna. 1 MW of applied power. a) In-phase operation, and b) out-of-phase operation.

Figure 7 Electron distribution that results for a parallel electric field of 5 V/cm and a shape factor, $s = 0.1$ cm.

Figure 8 Predicted change in T_e for three different shape factors along with the experimentally measured change in T_e. Prior to the ICRF, T_e was ~ 20 eV.

Figure 9 Quasilinear calculation of the electron distribution for an gap electric field of 2×10^{-4} V/cm. Also shown is a 20 eV Maxwellian. The curves have been normalized such that the number of particles are equal.

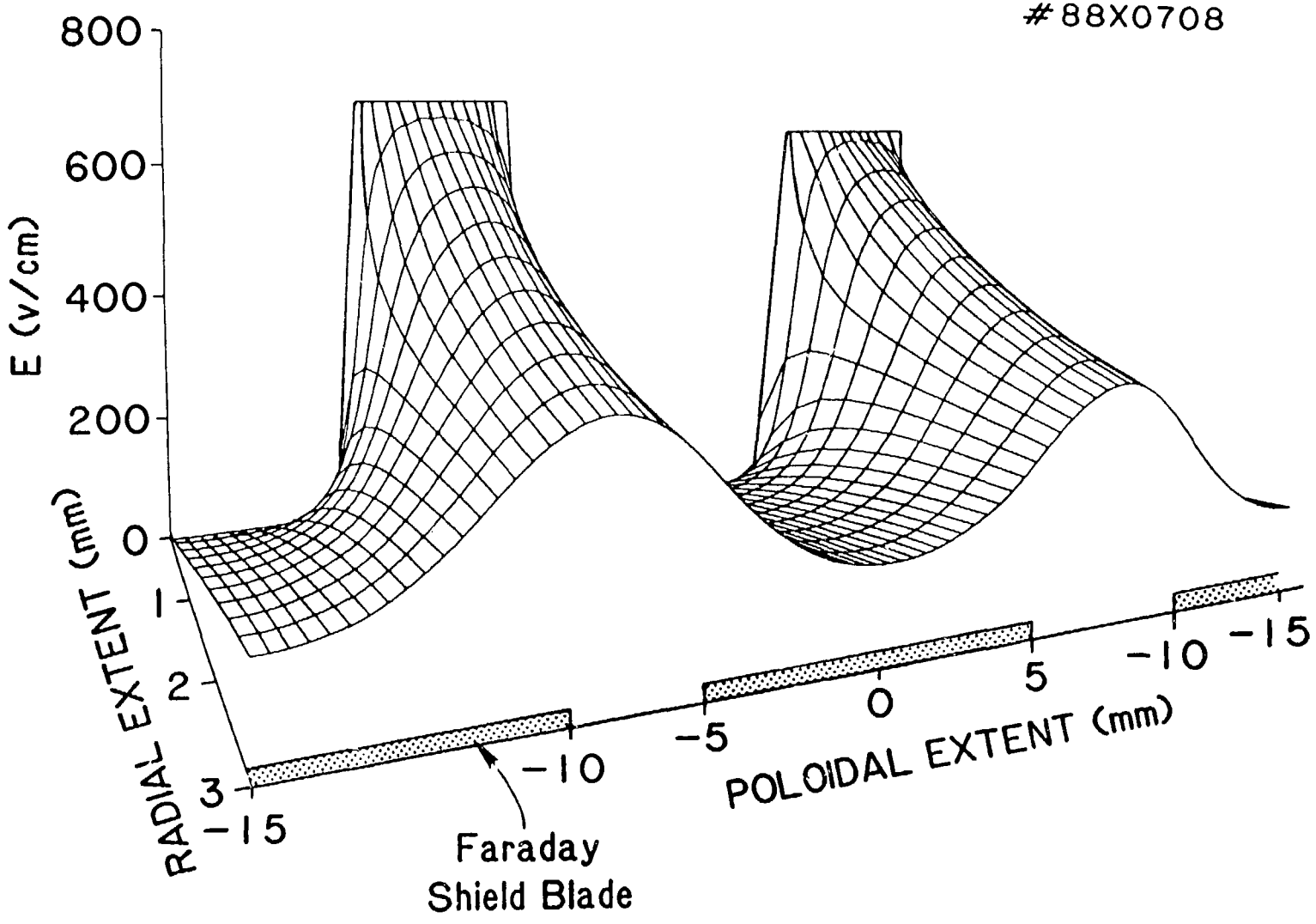
#88X0708
800
600
400
200
0
E (v/cm)
RADIAL EXTENT (mm)
1
2
3
-15
-10
-5
0
5
-10
-15
POLOIDAL EXTENT (mm)
Faraday
Shield Blade

Figure 1

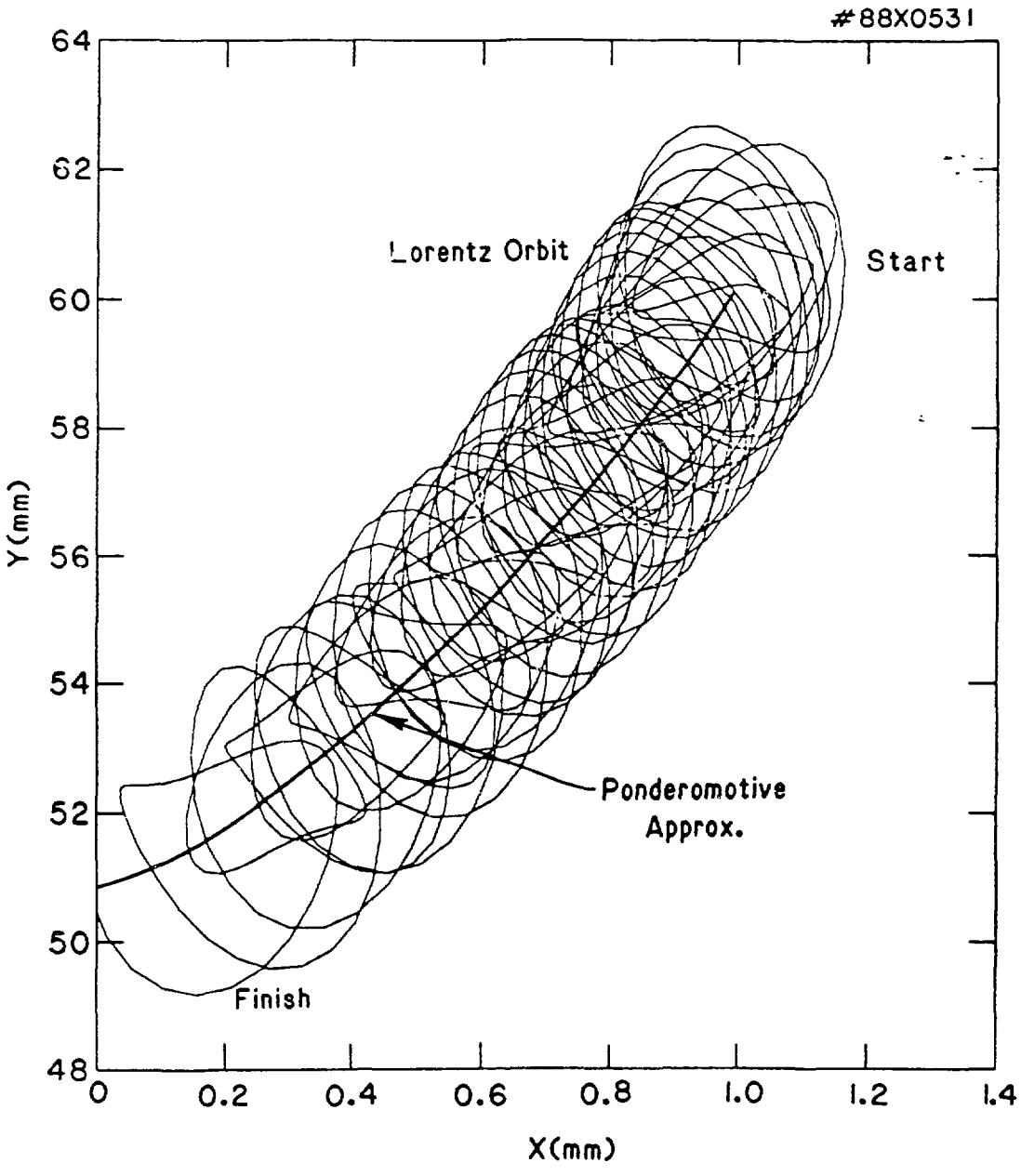
#88X0531
64
62
60
58
56
54
52
50
48
Y(mm)
0
0.2
0.4
0.6
0.8
1.0
1.2
1.4
X(mm)
Lorentz Orbit
Start
Ponderomotive
Approx.
Finish

Figure 2

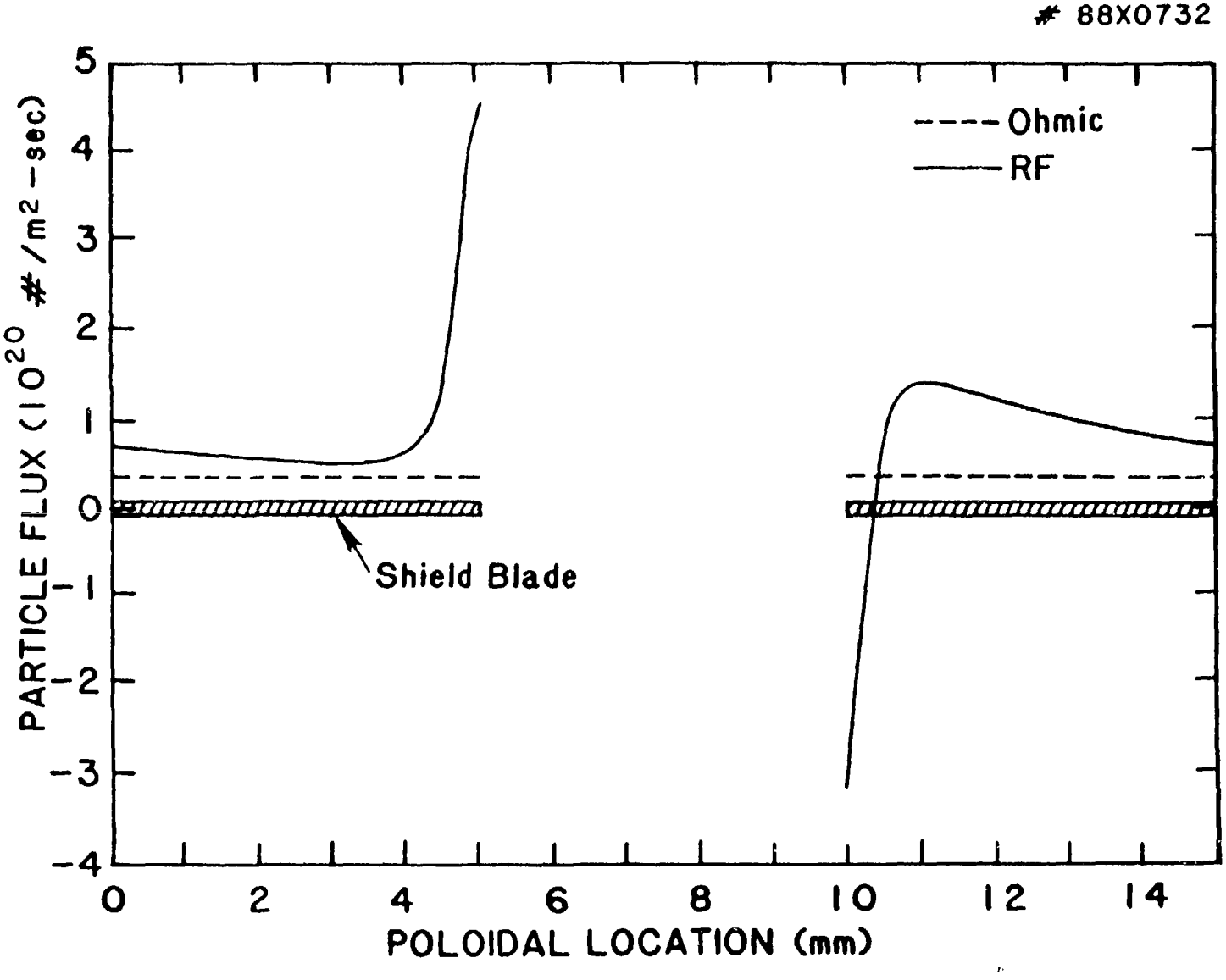
88X0732
Ohmic
RF
Shield Blade
PARTICLE FLUX (10^{20} #/m²-sec)
POLOIDAL LOCATION (mm)
5
4
3
2
1
0
-1
-2
-3
-4
0
2
4
6
8
10
12
14

Figure 3

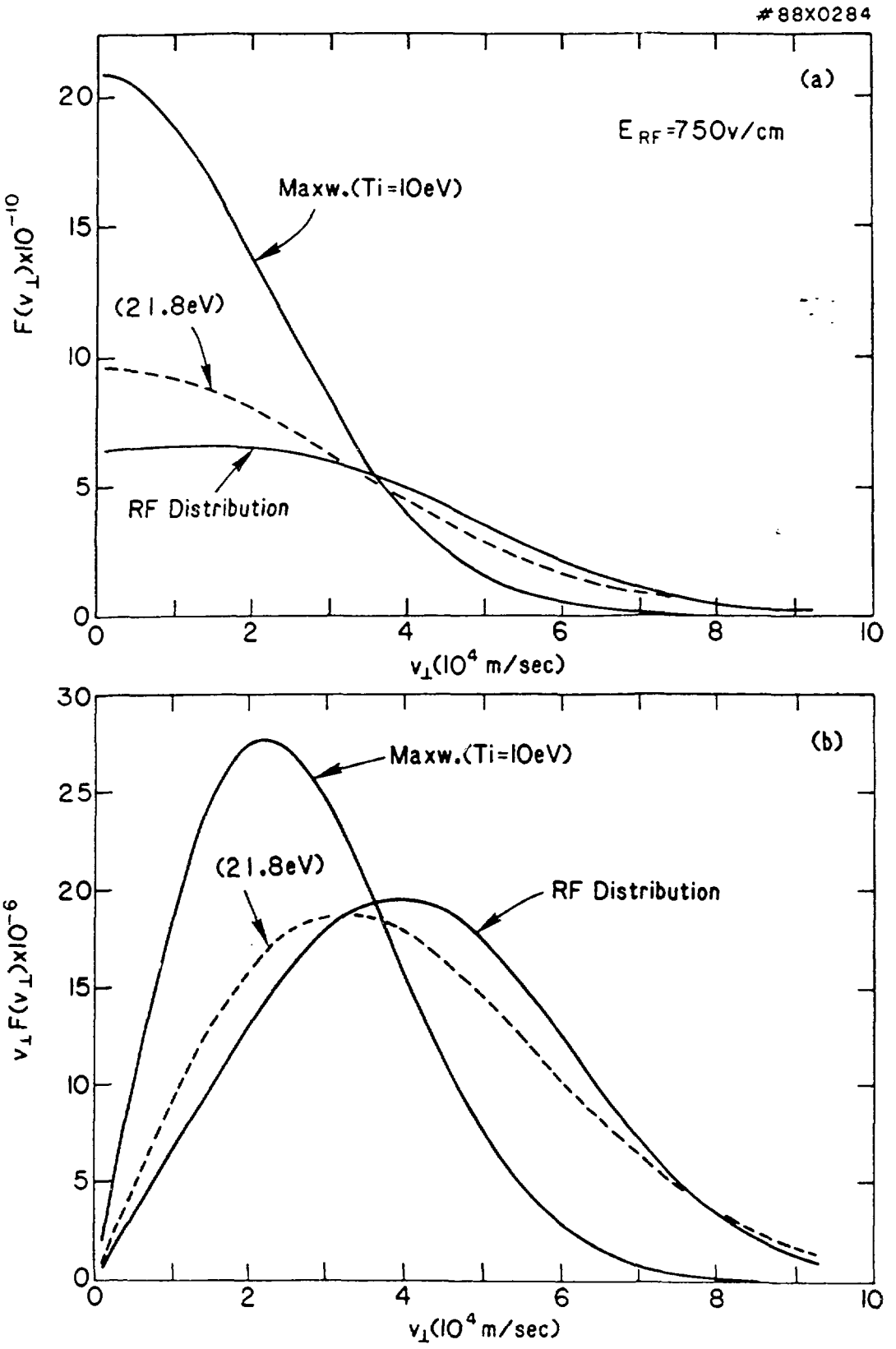
#88X0284
(a)
E_{RF}=750v/cm
Maxw.(Ti=10eV)
(21.8eV)
RF Distribution
$F(v_\perp)\times10^{-10}$
$v_\perp(10^4$ m/sec)
(b)
Maxw.(Ti=10eV)
(21.8eV)
RF Distribution
$v_\perp F(v_\perp)\times10^{-6}$
$v_\perp(10^4$ m/sec)

Figure 4

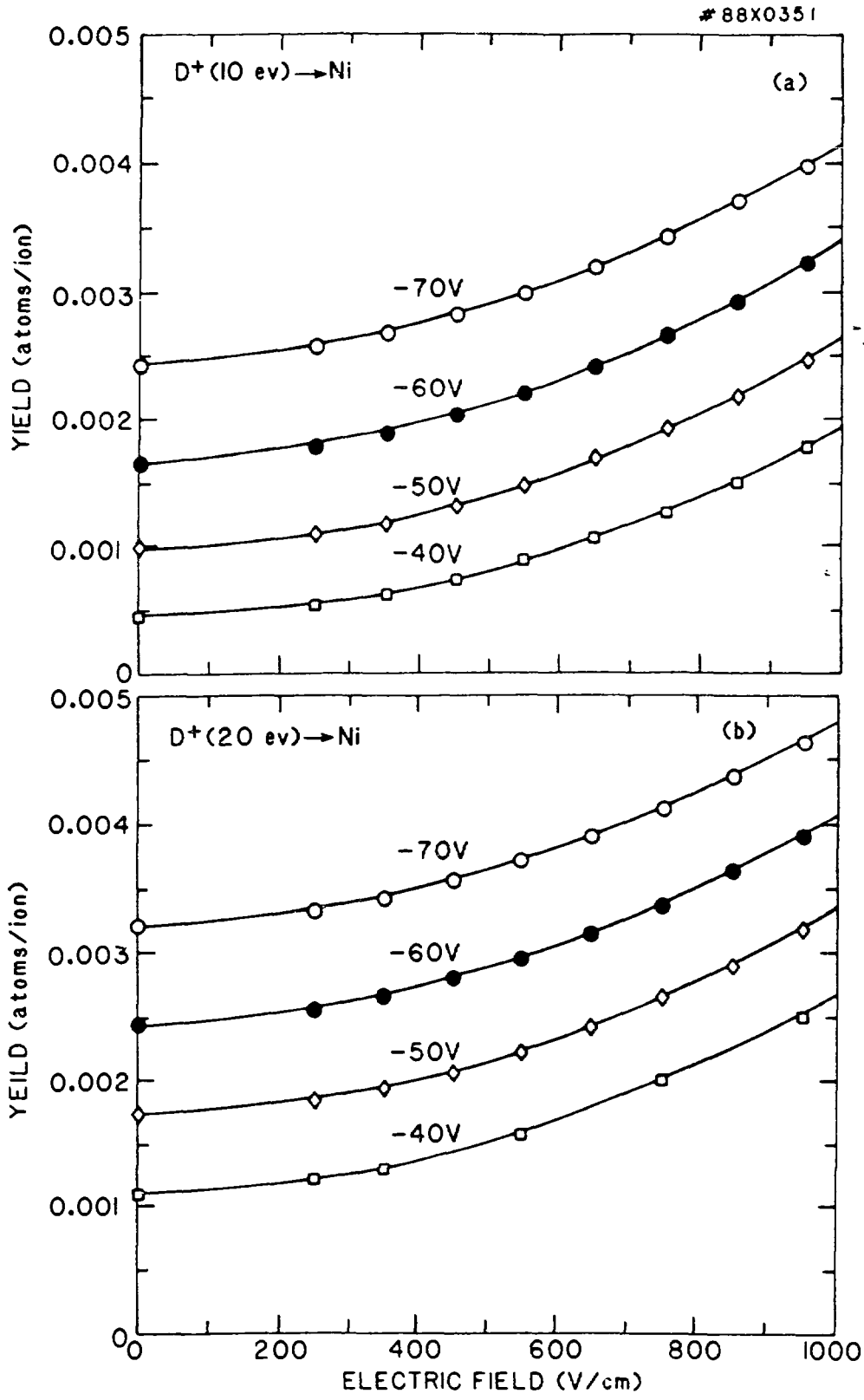
#88X0351
D+(10 ev)→Ni
(a)
-70V
-60V
-50V
-40V
YIELD (atoms/ion)
0.005
0.004
0.003
0.002
0.001
0
D+(20 ev)→Ni
(b)
-70V
-60V
-50V
-40V
YEILD (atoms/ion)
0.005
0.004
0.003
0.002
0.001
0
0
200
400
600
800
1000
ELECTRIC FIELD (V/cm)

Figure 5

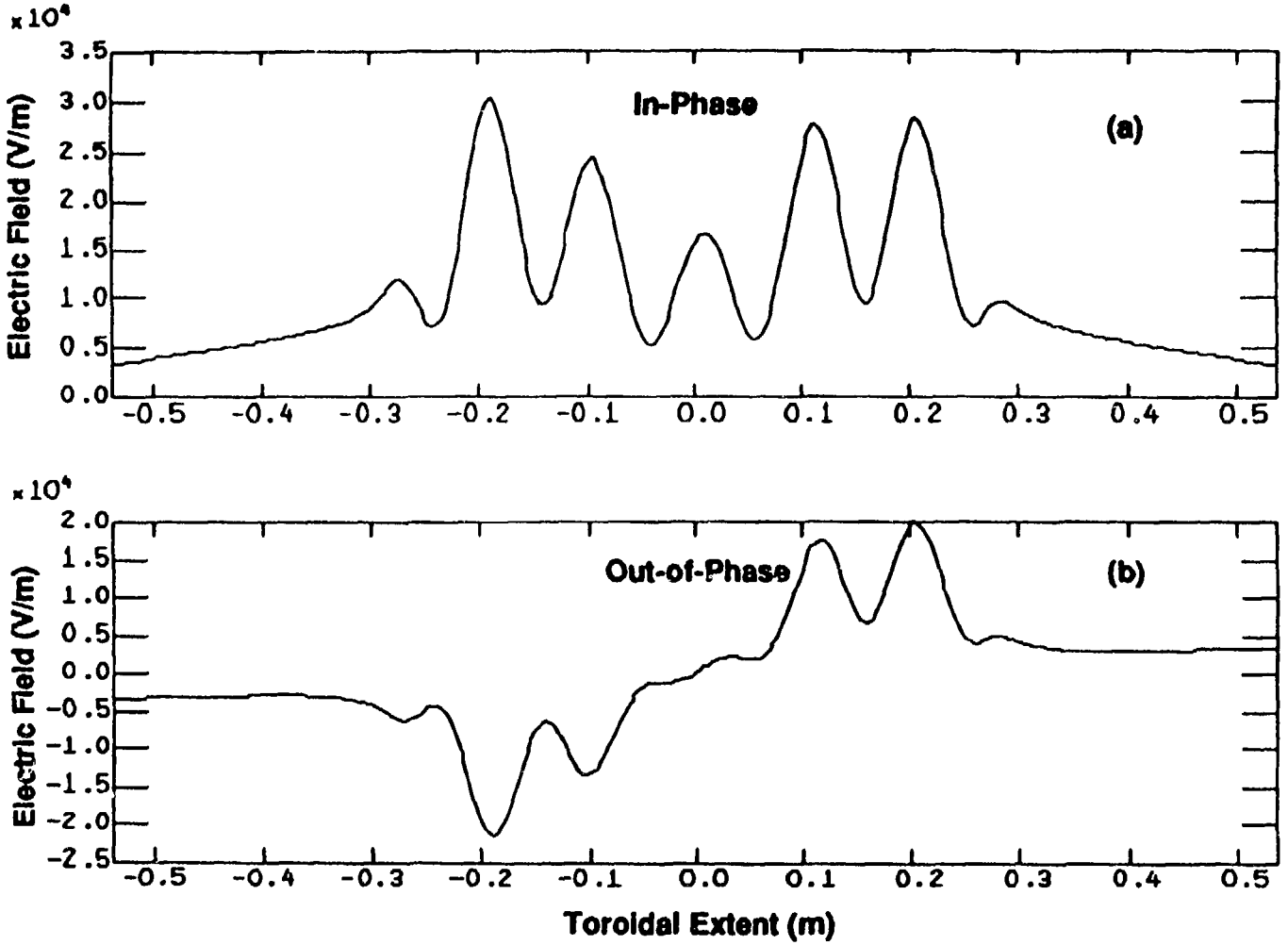
x10⁴
3.5
3.0
2.5
2.0
1.5
1.0
0.5
0.0
Electric Field (V/m)
In-Phase
(a)
-0.5 -0.4 -0.3 -0.2 -0.1 0.0 0.1 0.2 0.3 0.4 0.5
x10⁴
2.0
1.5
1.0
0.5
0.0
-0.5
-1.0
-1.5
-2.0
-2.5
Electric Field (V/m)
Out-of-Phase
(b)
-0.5 -0.4 -0.3 -0.2 -0.1 0.0 0.1 0.2 0.3 0.4 0.5
Toroidal Extent (m)

Figure 6

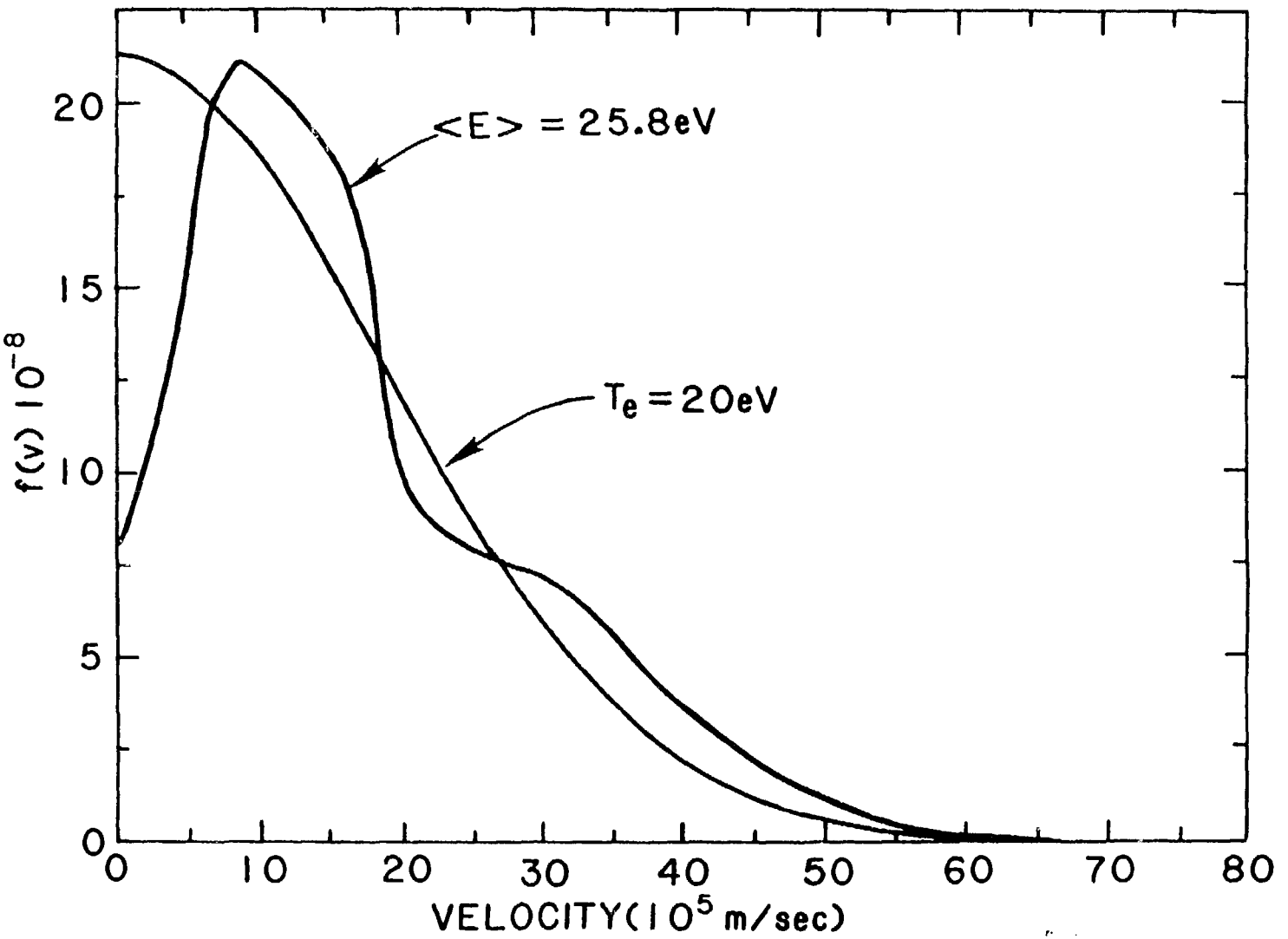
<E> = 25.8eV
T_e = 20eV
f(v) 10^{-8}
VELOCITY(10^5 m/sec)
0
5
10
15
20
0
10
20
30
40
50
60
70
80

Figure 7

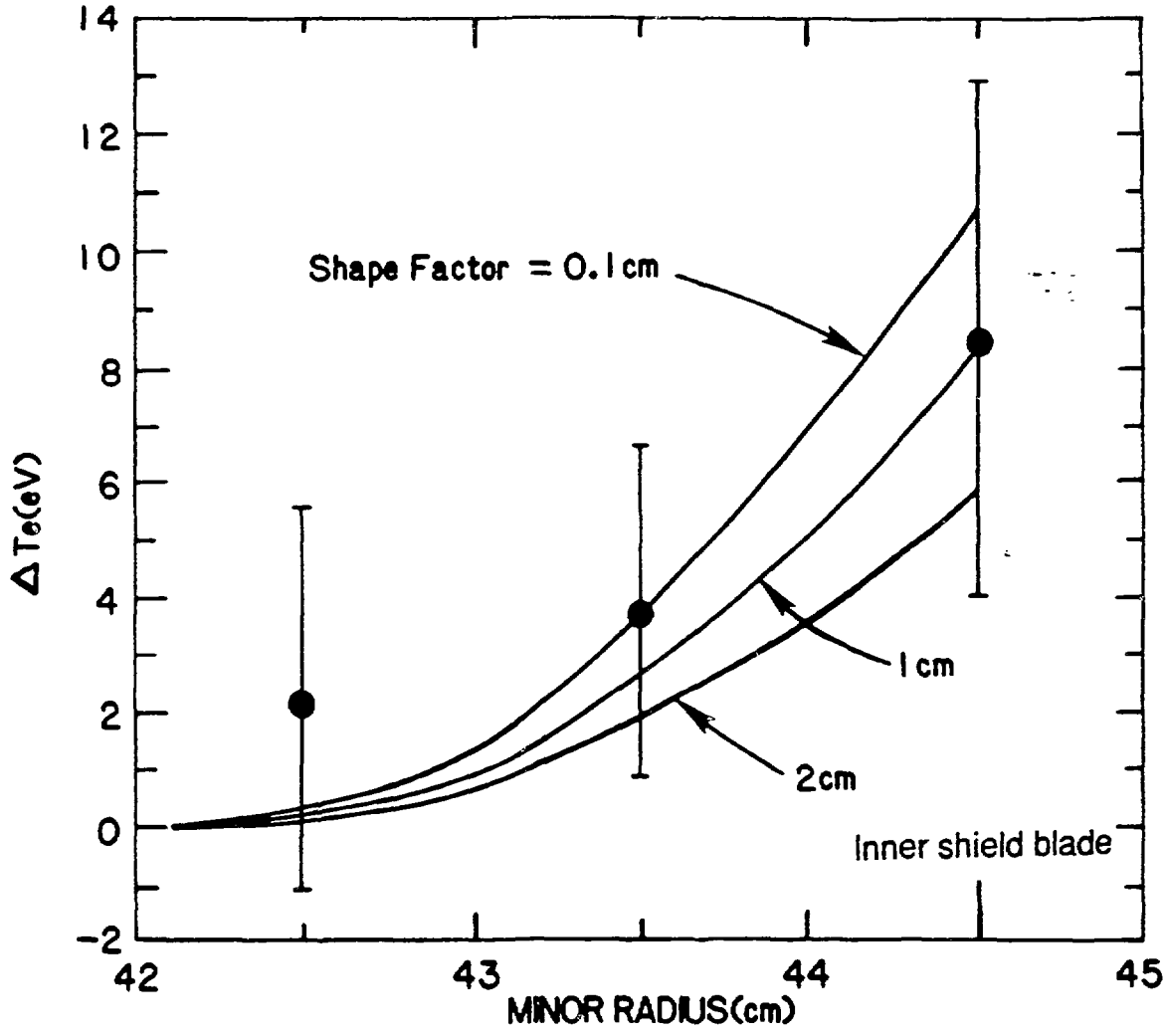
14
12
10
8
6
4
2
0
-2
ΔTe(eV)
Shape Factor = 0.1cm
1cm
2cm
Inner shield blade
42
43
44
45
MINOR RADIUS(cm)

Figure 8

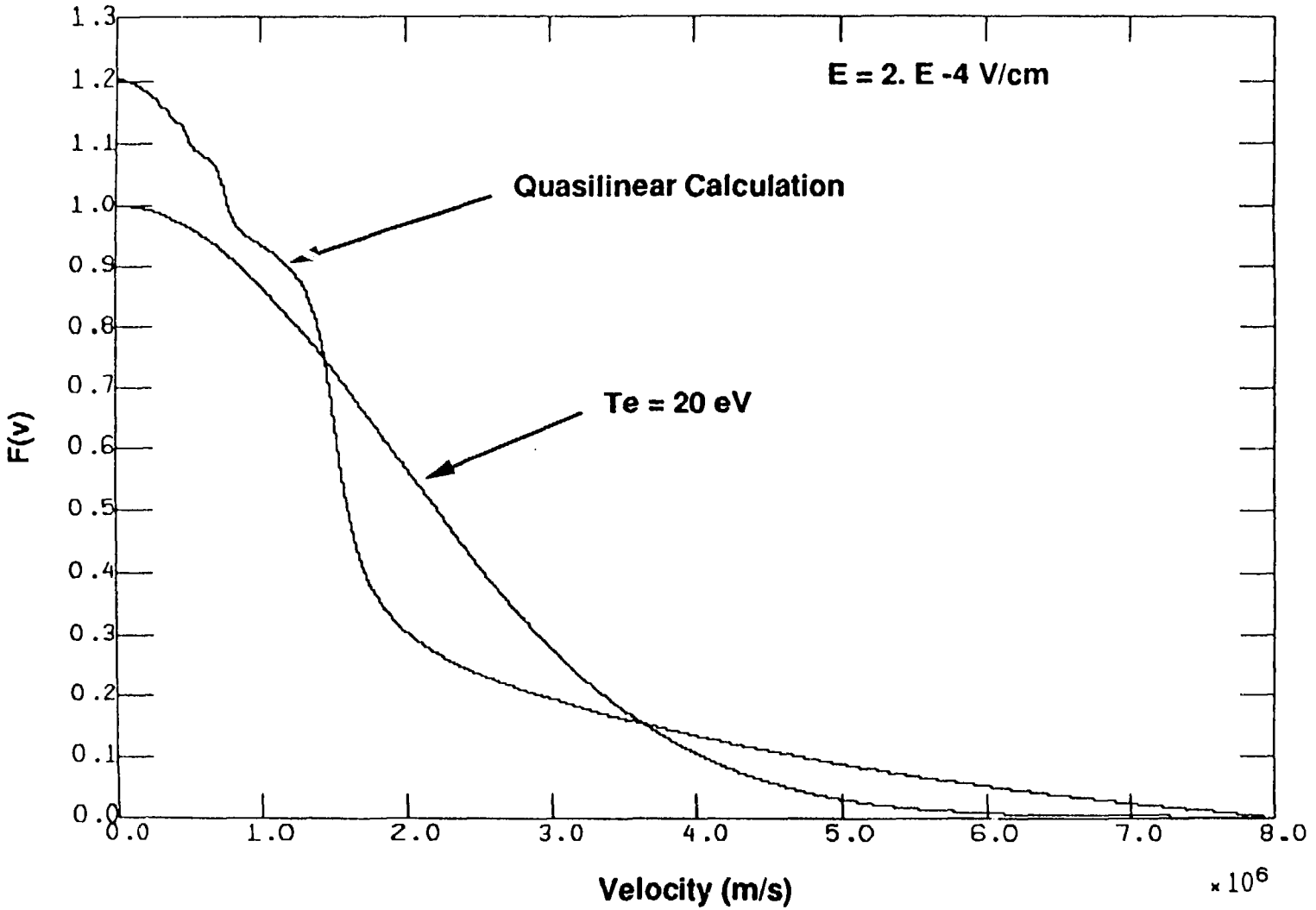
E = 2. E -4 V/cm
Quasilinear Calculation
Te = 20 eV
F(v)
Velocity (m/s)
x 10^6
1.3
1.2
1.1
1.0
0.9
0.8
0.7
0.6
0.5
0.4
0.3
0.2
0.1
0.0
0.0
1.0
2.0
3.0
4.0
5.0
6.0
7.0
8.0

Figure 9